Thermal dilepton rates from quenched lattice QCD

O. Kaczmarek, E. Laermann, M. Müller[*]

Fakultät für Physik, Universität Bielefeld, D-33615 Bielefeld, Germany
E-mail: okacz, edwin, mmueller@physik.uni-bielefeld.de

F. Karsch

Fakultät für Physik, Universität Bielefeld, D-33615 Bielefeld, Germany
Physics Department, Brookhaven National Laboratory, Upton, NY 11973, USA
E-mail: karsch@quark.phy.bnl.gov

H.-T. Ding, S. Mukherjee

Physics Department, Brookhaven National Laboratory, Upton, NY 11973, USA
E-mail: htding, swagato@quark.phy.bnl.gov

A. Francis

Institut für Kernphysik, Johannes Gutenberg-Universität Mainz, D-55099 Mainz, Germany
E-mail: francis@kph.uni-mainz.de

W. Soeldner

Fakultät für Physik, Universität Regensburg, D-93053 Regensburg, Germany
E-mail: wolfgang.soeldner@physik.uni-regensburg.de

We present new lattice results on the continuum extrapolation of the vector current correlation function. Lattice calculations have been carried out in the deconfined phase at a temperature of $T = 1.1T_c$, extending our previous results at $T = 1.45T_c$, utilizing quenched non-perturbatively clover-improved Wilson fermions and light quark masses. A systematic analysis on multiple lattice spacings allows to perform the continuum limit of the correlation function and to extract spectral properties in the continuum limit.

Our current analysis suggests the results for the electrical conductivity are proportional to the temperature and the thermal dilepton rates in the quark gluon plasma are comparable for both temperatures. Preliminary results of the continuum extrapolated correlation function at finite momenta, which relates to thermal photon rates, are also presented.

Xth Quark Confinement and the Hadron Spectrum,
October 8-12, 2012
TUM Campus Garching, Munich, Germany

[*]Speaker.

1. Introduction

Current Heavy-Ion-experiments at LHC and RHIC reach energies in a region where the transition from normal nuclear matter to a quark gluon plasma occurs. In this phase thermally produced dileptons and photons are important experimental observables. To understand their yields, hydrodynamic models for the evolution of the medium need detailed knowledge of the dilepton and photon rates as well as the transport coefficients during the evolution of the system [1]. These require non-perturbative ab initio lattice QCD calculations as input.

On the lattice, hadronic correlation functions for different particle channels can be calculated at zero and at fixed finite temperatures. From the vector spectral function the electrical conductivity and the dilepton rates of the medium can be extracted. The spectral function has recently been extracted by employing phenomenologically inspired ansätze [2, 3].

Our previous work on dilepton rates provided the first results for a continuum extrapolation of the vector meson correlation at a temperature of $T/T_c = 1.45$ and light quark masses [4]. An ansatz for the spectral function could successfully be used to describe this dataset, thereby the dilepton rate could be obtained at a first relevant temperature. Together with results for the electrical conductivity at different temperatures $1.16 < T/T_c < 2.98$ [5] this motivated the systematic study of the temperature dependence of the vector spectral function on the lattice. For results using two dynamical flavors at finite lattice spacings see [6].

The work presented here extends the continuum extrapolated quenched calculations to a second relevant temperature $T/T_c = 1.1$.

2. Thermal vector correlator and spectral function

2.1 Vector correlation function

The Euclidean time two-point correlation function $G(\tau, \vec{p})$ of the vector current J_μ is a quantity directly accessible in lattice QCD calculations,

$$G_{\mu\nu}(\tau, \vec{p}) = \int d^3x J_\mu(\tau, \vec{x}) J_\nu^\dagger(0, \vec{0}) e^{i\vec{p}\vec{x}} \quad \text{with} \quad J_\mu(\tau, \vec{x}) = \bar{q}(\tau, \vec{x})\gamma_\mu q(\tau, \vec{x}). \tag{2.1}$$

Only contributions of quark line connected diagrams are included. Disconnected diagrams cause a high numerical effort, but are expected to be small in the high temperature phase of QCD [7, 8]. The correlation function directly relates to the spectral function via

$$G_H(\tau, \vec{p}, T) = \int_0^\infty \frac{d\omega}{2\pi} \rho_H(\omega, \vec{p}, T) \frac{\cosh(\omega(\tau - 1/2T))}{\sinh(\omega/2T)} \quad \text{with:} \quad H = 00, ii, V. \tag{2.2}$$

Here ρ_{ii} denotes a sum over the spatial components, while ρ_{00} denotes the time-like components. The full vector spectral function is denoted by $\rho_V = \rho_{00} + \rho_{ii}$. As lattice QCD calculations are carried out at a fixed temperature, the explicit temperature dependence of ρ is dropped and observables are usually given in units of the temperature T.

2.2 Ansatz for the spectral function

The time-like component of the vector correlator G_{00} and thereby the corresponding transformation of the spectral function ρ_{00} is related to the quark number susceptibility χ_q. Since the quark

number is conserved, the correlator is constant in (here Euclidean) time, $G_{00}(\tau T) = -\chi_q T$ and its spectral representation is given by a delta function

$$\rho_{00}(\omega) = -2\pi\chi_q\omega\delta(\omega). \tag{2.3}$$

The spatial components of the spectral functions increase quadratically for large values of ω, in the free field limit for massless quarks to

$$\rho_{ii}^{\text{free}}(\omega) = 2\pi T^2\omega\delta(\omega) + \frac{3}{2\pi}\omega^2\tanh(\omega/4T). \tag{2.4}$$

In this limit, the delta peak in the spatial and the time-like component of the spectral function cancel. In the interacting theory however, this is not the case: The time-like component maintains a delta peak since it is linked to the conserved current. In the spatial component however the delta peak is smeared out and expected to be described by a Breit-Wigner peak [9, 10, 11, 12]

$$\rho_{ii}^{\text{interac.}}(\omega) = \chi_q c_{\text{BW}}\frac{\omega\Gamma}{\omega^2 + (\Gamma/2)^2} + (1+\kappa)\frac{3}{2\pi}\omega^2\tanh(\omega/4T). \tag{2.5}$$

This ansatz leaves three parameters, the strength (c_{BW}) and width (Γ) of the Breit-Wigner peak as well as κ, which accounts for the deviation from free theory. The relation of this ansatz to the correlator obtained on the lattice is given by (2.2).

The fits are not performed directly to the correlation function G_{ii} but to a set of two ratios: The correlation function is normalized by the quark number susceptibility (as given in (2.3)), resulting in a dimensionless quantity independent of renormalization constants. It is also normalized by the free field correlation function $G_V^{\text{free}}(\tau T)$, yielding a smooth function that does not fall off over multiple decades like the correlation function. Furthermore, due to asymptotic freedom, the correlation function approaches the non-interacting limit at asymptotically small distances. The spectral function is thereby fitted to reproduce

$$\frac{G_{ii}(\tau T)/G_{00}}{G_V^{\text{free}}(\tau T)/G_{00}^{\text{free}}}. \tag{2.6}$$

Having obtained the spectral function, relevant properties of the medium can be calculated, e.g. the electrical conductivity as

$$\frac{\sigma}{T} = \frac{C_{\text{em}}}{6}\lim_{\omega\to 0}\frac{\rho_{ii}(\omega)}{\omega T} \quad \to \quad \sigma(T)/C_{\text{em}} = 2\chi_q c_{\text{BW}}/(3\Gamma) \tag{2.7}$$

where C_{em} is given by the elementary charges Q of the quark flavor f as $C_{\text{em}} = \sum_f Q_f^2$, and the thermal production rate of dilepton pairs as

$$\frac{dW}{d\omega d^3 p} = \frac{5\alpha^2}{54\pi^3}\frac{1}{\omega^2(e^{\omega/T}-1)}\rho_{ii}(\omega, p, T). \tag{2.8}$$

2.3 Thermal moments

Using the ansatz above to perform a three-parameter fit of the spectral function, the Breit-Wigner parameters are most sensitive to the low ω region, thereby to the large distance behavior of the correlator.

N_τ	N_σ	β	κ	$1/a[\text{GeV}]$	$a[\text{fm}]$	#conf
32	96	7.192	0.13440	9.65	0.020	314
48	144	7.544	0.13383	14.21	0.015	315
64	192	7.793	0.13345	19.30	0.010	242

Table 1: Summary of simulation parameters

This region of the correlator can be further constrained by calculating the curvature of the correlator for large Euclidean distances τT. The thermal moments

$$G_H^{(n)} = \frac{1}{n!} \frac{d^n G_H(\tau T)}{d(\tau T)^n}\bigg|_{\tau T=1/2} = \frac{1}{n!} \int_0^\infty \frac{d\omega}{2\pi} \left(\frac{\omega}{T}\right)^n \frac{\rho_H(\omega)}{\sinh(\omega/2T)} \quad \text{with} \quad H = ii, V \qquad (2.9)$$

are given as the Taylor coefficients of the correlation function expanded around the midpoint

$$G_H(\tau T) = \sum_{n=0}^\infty G_H^{(2n)} \left(\frac{1}{2} - \tau T\right)^{2n}. \qquad (2.10)$$

For the infinite temperature, free field limit, the thermal moments can be calculated analytically. For the analysis, the ratios of interacting to free midpoint subtracted correlation functions,

$$\Delta_V(\tau T) = \frac{G_V(\tau T) - G_V^{(0)}}{G_V^{\text{free}}(\tau T) - G_V^{(0),\text{free}}} = \frac{G_V^{(2)}}{G_V^{(2),\text{free}}} \left(1 + (R_V^{(4,2)} - R_{V,\text{free}}^{(4,2)})(\frac{1}{2} - \tau T)^2 + \ldots\right), \qquad (2.11)$$

have been calculated, where $R_V^{(n,m)} = G_V^{(n)}/G_V^{(m)}$. The first two terms (up to quadratic) are then used in the fit.

For the $1.45T_c$ dataset, restricting the spectral function fit to also reproduce these first two thermal moments allowed to obtain a stable fit. Since the new $1.1T_c$ dataset allows for a more precise continuum extrapolation down to a distance $\tau T_{\min} = 0.15$, which is smaller than the distance $\tau T_{\min} = 0.25$ reachable at $1.45T_c$, we find that stable fits at this temperature (giving results within the systematic errors of this analysis) can also be performed without including the thermal moments as an additional constraint.

3. Results for correlators and spectral function fits

Vector correlators are obtained on lattices of size $N_\sigma^3 \times N_\tau$, where for the new dataset at $1.1T_c$ three fixed lattice spacings $(aT)^{-1} = N_t = 32, 48, 64$ where chosen for the continuum extrapolation. For each size β was set to match the fixed temperature and κ was tuned to light quark masses (see table 1). From the previous study at $1.45T_c$, finite volume effects are found to be small for a fixed aspect ratio $N_\sigma/N_\tau = 3$, so the lattice sizes were set to $96^3 \times 32$, $144^3 \times 48$ and $192^3 \times 64$.

Cut-off effects are removed by a continuum extrapolation of the correlators: Discretization errors of non-perturbatively clover-improved Wilson fermions have a quadratic error in the lattice spacing allowing to extrapolate the correlators in a^2, corresponding to $1/N_\tau^2$ at fixed temperature
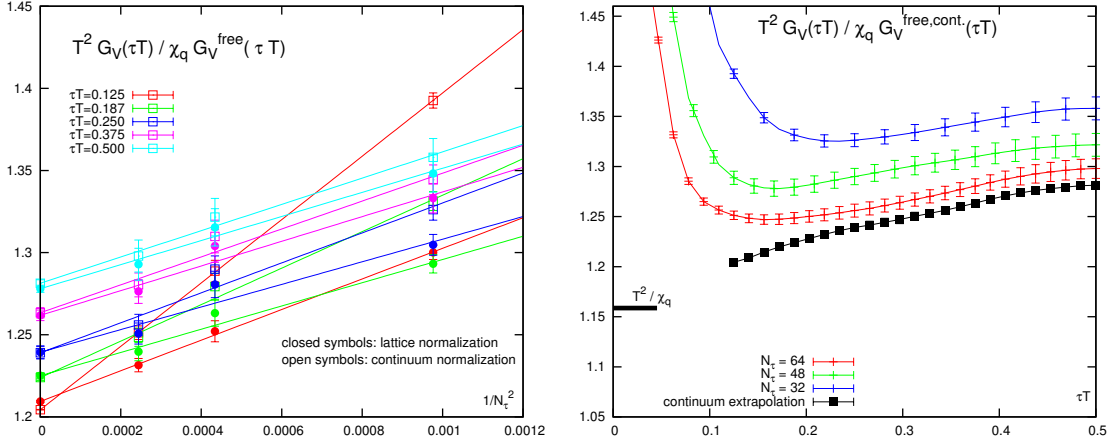
Figure 1: *Left:* Continuum extrapolation of the correlator ratio $G_V(\tau T)/G_V^{\text{free,lat.}}(\tau T)$ and $G_V(\tau T)/G_V^{\text{free,cont.}}(\tau T)$ at different time-like separations τT. Cutoff effects are under control for $0.125 < \tau T < 0.5$. *Right:* Correlator ratio $G_V(\tau T)/G_V^{\text{free,cont.}}(\tau T)$ for the three lattice spacings and continuum extrapolation.

T. For these extrapolations, the ratios (2.6) of the interacting correlators to free theory are used. On the coarser lattices these ratios are spline-interpolated to provide every spacing τT present in the finest correlator. As can be seen in figure 1, calculating ratios to the free continuum as well as to the free lattice correlators give the same continuum extrapolation for Euclidean time separations $\tau T > 0.125$ and the results show that lattice cutoff effects are under control in the region $0.15 < \tau T < 0.5$.
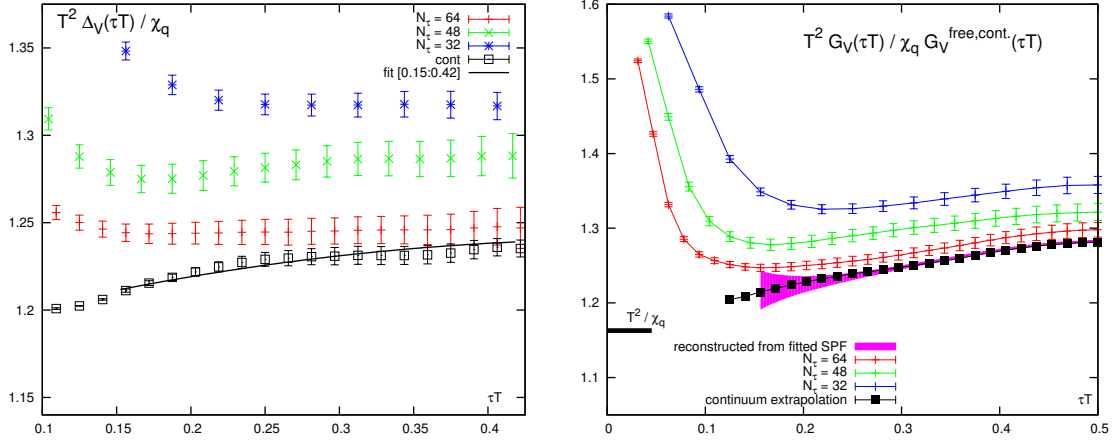
3.1 Fitting the spectral function

After the continuum extrapolation of the vector correlation function has been obtained, the first and second thermal moments are computed by fitting the curvature of the midpoint subtracted correlator (2.11). Both the correlator ratio $G_V(\tau T)/\chi_q G_V^{\text{free}}(\tau T)$ and the ratio of the first thermal moments serve as input and constraints for a fit of the parameters c_{BW}, Γ, κ in the spectral function ansatz (2.5) to reproduce the correlator (2.2). As can be seen in figure 2 (right), the fitted spectral function reproduces the correlation functions. The thermal moments constrain the small ω region, so errors of the spectral function fit descrese with increasing τT.

3.2 Breit-Wigner with truncated continuum

As in the analysis of the $1.45T_c$ dataset [4], to study the systematic uncertainties of our Ansatz for the spectral function the low energy structure of the spectral function was studied by smoothly cutting the continuum contribution at a frequency ω_0 with a width of Δ_ω

$$\rho_{ii}^{\text{trunc.}}(\omega) = \chi_q c_{\text{BW}} \frac{\omega \Gamma}{\omega^2 + (\Gamma/2)^2} + (1+\kappa)\frac{3}{2\pi}\omega^2 \tanh(\omega/4T)\Theta(\omega_0, \Delta_\omega) \tag{3.1}$$

$$\text{with} \quad \Theta(\omega_0, \Delta_\omega) = \left(1 + e^{(\omega_0^2 - \omega^2)/\omega\Delta_\omega}\right)^{-1}$$

Figure 2: *Left:* Ratio of midpoint substracted correlators $(G_V(\tau T) - G_V^{(0)})/(G_V^{\text{free}}(\tau T) - G_V^{(0),\text{free}})$, including a fit of the curvature (2.11) and thereby the thermal moments. *Right:* Fit of the continuum extrapolated correlator to (2.2) with the spectral function ansatz (2.5).

The fit with (3.1) is performed for a range of values ω_0 and Δ_ω. The systematic errors given in figure 3 correspond to the minimal and maximal values c_{BW} found in these fits with $\chi^2/\text{d.o.f} < 1.1$, thereby giving a minimal and maximal electrical conductivity (2.7) within this framework.

From the corresponding spectral functions the dilepton rates shown in figure 3 (right) are calculated (2.8). Within the current systematic uncertainties, the dilepton rates and electrical conductivities in units of T agree between $1.1 T_c$ and $1.45 T_c$. This linear temperature dependence of the electrical conductivity is in agreement with the results of [13].

In order to study systematic errors, also a variation of the ansatz (3.1) motivated by Operator Product Expansion [14] can be used. First tests show only small deviations that are well within the systematic errors between both version of the ansatz.

## 4. Outlook: Correlation functions at finite momenta

Extracting the spectral function at vanishing momentum $\vec{p} = 0$ gives access to the dilepton rates and the electric conductivity. For finite momenta $\vec{p} \neq 0$ the correlation and spectral functions split into a longitudinal and transversal part, where the transversal ρ_T relates to the photon rate:

$$\omega \frac{dR_\gamma}{d^3 p} \sim \frac{\rho_T(\omega = |\vec{p}|, T)}{\exp(\omega/T) - 1}. \tag{4.1}$$

On the lattice, only a finte number of discrete momenta are accessible, the momenta are given by the aspect ratio N_σ/N_τ and a vector of integer numbers $\vec{k}$ as $\vec{p}/T = 2\pi \cdot \vec{k} \cdot N_\tau/N_\sigma$. All $1.1 T_c$ correlator calculations have been performed on the same aspect ratio of $N_\sigma/N_\tau = 3$, so a continuum extrapolation of the correlator at fixed momenta can be performed. As can be seen in figure 4, this extrapolation is well behaved as in the zero momentum case and gives precise results for the vector correlation function at finite momentum $\vec{p}$ in the continuum limit. Work on the extraction of the corresponding spectral functions and the determination of the photon rate is in progress.
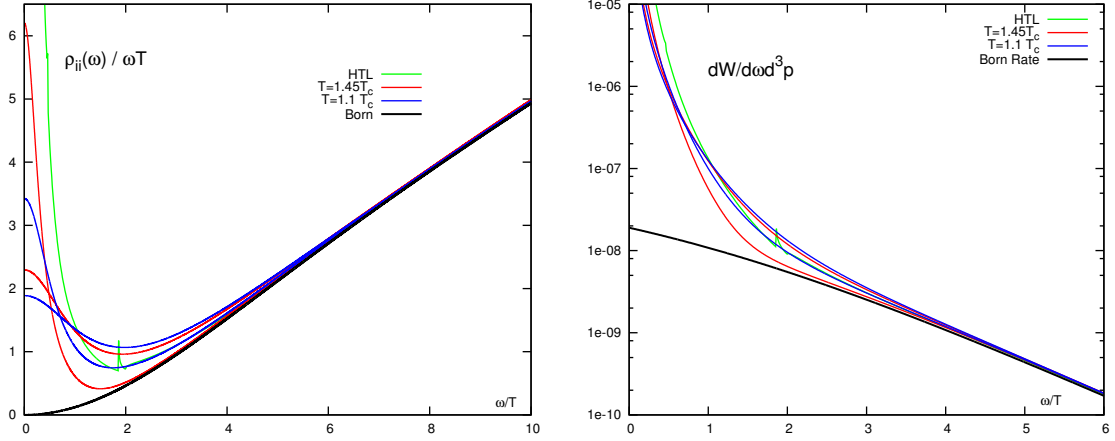
Figure 3: *Left:* Spectral function as fitted to the vector correlation function. Two lines are shown for each temperature as a result of the systematic error estimation, given by the two ρ_{ii} with the minimal and maximal c_{BW} that can be obtain via the Breit-Wigner + truncated continuum ansatz (3.1), while maintaining a $\chi/\mathrm{d.o.f} < 1.1$ in the fit. Results from the hard thermal loop resummation scheme (HTL) are also included in the plot [15]. *Right:* Thermal dilepton rate calculated from the spectral function (2.8).
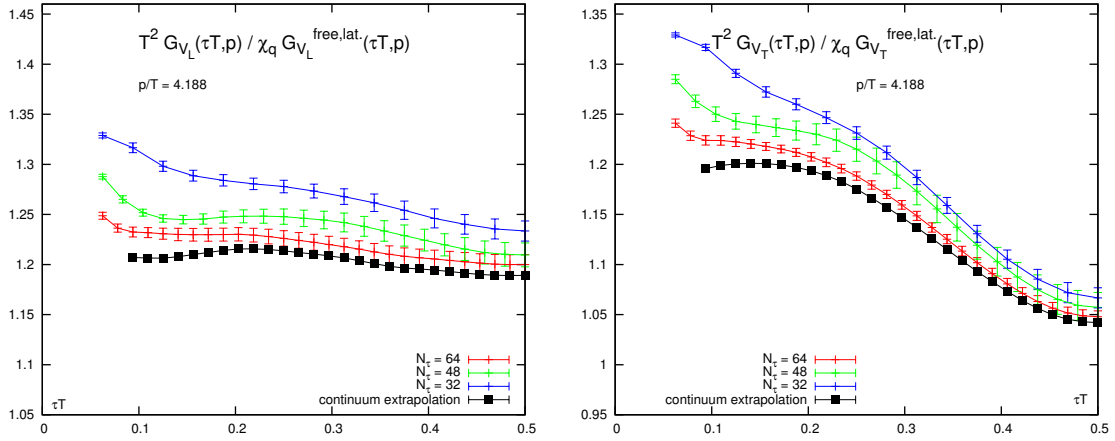
Figure 4: Continuum extrapolation of the logitudinal (left) and transversal (right) vector correlation function G_V/G_V^{free} at non-zero momentum.

5. Conclusion

Lattice calculations of the vector correlation function have been performed for two temperatures in the deconfined phase of QCD. Calculations at different lattice spacings were used for a successfull continuum extrapolation to remove cut-off effects. Using a phenomenologically motivated ansatz, the vector spectral function to the continuum-extrapolated correlation function was obtained, giving access to the dilepton rate and the electric conductivity of the medium at the given temperatures. Within current systematic uncertainties, the electric conductivity divided by temperature and the thermal dilepton rates are are compatible at $1.1T_c$ and $1.45T_c$. A continuum extrapolation was also performed for the correlation functions at a range of finite momenta, opening

the possibility to study the photon rate in the future.

6. Acknowlegdements

References

[1] R. Rapp, J. Wambach, and H. van Hees, *The Chiral Restoration Transition of QCD and Low Mass Dileptons*, in *Landolt-Börnstein*, vol. I-23, 4-1. Springer-Verlag, 2010. `arXiv:0901.3289`.

[2] O. Kaczmarek, *Recent Developments in Lattice Studies for Quarkonia*, to appear in *Nucl. Phys. A* [`arXiv:1208.4075`].

[3] H.-T. Ding, *In-medium hadron properties from lattice qcd*, *EPJ Web of Conferences* **36** (2012) 00008, [`arXiv:1207.5187`].

[4] H.-T. Ding, A. Francis, O. Kaczmarek, F. Karsch, E. Laermann, et al., *Thermal dilepton rate and electrical conductivity: An analysis of vector current correlation functions in quenched lattice QCD*, *Phys.Rev.* **D83** (2011) 034504, [`arXiv:1012.4963`].

[5] A. Francis and O. Kaczmarek, *On the temperature dependence of the electrical conductivity in hot quenched lattice QCD*, *Prog.Part.Nucl.Phys.* **67** (2012) 212–217, [`arXiv:1112.4802`].

[6] B. B. Brandt, A. Francis, H. B. Meyer, and H. Wittig, *Thermal Correlators in the ρ channel of two-flavor QCD*, `arXiv:1212.4200`.

[7] C. Allton, M. Doring, S. Ejiri, S. Hands, O. Kaczmarek, et al., *Thermodynamics of two flavor QCD to sixth order in quark chemical potential*, *Phys.Rev.* **D71** (2005) 054508, [`hep-lat/0501030`].

[8] R. V. Gavai, S. Gupta, and P. Majumdar, *Susceptibilities and screening masses in two flavor QCD*, *Phys.Rev.* **D65** (2002) 054506, [`hep-lat/0110032`].

[9] G. Aarts and J. M. Martinez Resco, *Transport coefficients, spectral functions and the lattice*, *JHEP* **0204** (2002) 053, [`hep-ph/0203177`].

[10] G. D. Moore and J.-M. Robert, *Dileptons, spectral weights, and conductivity in the quark-gluon plasma*, `hep-ph/0607172`.

[11] P. Petreczky and D. Teaney, *Heavy quark diffusion from the lattice*, *Phys.Rev.* **D73** (2006) 014508, [`hep-ph/0507318`].

[12] J. Hong and D. Teaney, *Spectral densities for hot QCD plasmas in a leading log approximation*, *Phys.Rev.* **C82** (2010) 044908, [`arXiv:1003.0699`].

[13] G. Aarts, C. Allton, J. Foley, S. Hands, and S. Kim, *Spectral functions at small energies and the electrical conductivity in hot, quenched lattice QCD*, *Phys.Rev.Lett.* **99** (2007) 022002, [`hep-lat/0703008`].

[14] Y. Burnier and M. Laine, *Towards flavour diffusion coefficient and electrical conductivity without ultraviolet contamination*, *Eur.Phys.J.* **C72** (2012) 1902, [`arXiv:1201.1994`].

[15] E. Braaten and R. D. Pisarski, *Soft Amplitudes in Hot Gauge Theories: A General Analysis*, *Nucl.Phys.* **B337** (1990) 569.